J Mater Sci (2011) 46:6700–6708
DOI 10.1007/s10853-011-5623-4

Modeling of the wear behavior in A356–B_4C composites

Mohsen Ostad Shabani · Ali Mazahery

Received: 14 February 2011 / Accepted: 9 May 2011 / Published online: 26 May 2011

Abstract In this study, attempts were made to coat the boron carbide (B_4C) powders with TiB_2 via a sol–gel process. Different volume fraction of coated B_4C particles were incorporated into the aluminum alloy by a mechanical stirrer and wear properties of unreinforced A356 alloy and composites with different vol% of coated B_4C particles were experimentally investigated. Further study was carried out on the performance of artificial neural network (ANN) in prediction of the composites wear behavior. The finite element technique was implemented to obtain two of the inputs, cooling rate and temperature gradient. It is observed that predictions of ANN are consistent with experimental measurements for A356 composite and considerable savings in terms of cost and time could be obtained by using neural network model.

Introduction

A vast range of metal matrix composite (MMC) materials has been conceived and studied to combine the desirable attributes of metal and ceramics. The addition of high strength, high modulus refractory particles to a ductile metal matrix produce a material whose mechanical properties are intermediate between the matrix alloy and ceramic reinforcement. Matrices based on Ag, Al, Be, Co, Cu, Fe, Mg, Ni, and Ti are all commercially produced and used. By far the largest commercial volumes are for aluminum matrix composites (AMCs), which accounts for 69% of the annual MMC production by mass [1–6]. The wear resistance of aluminum alloys is also improved as a consequence of the incorporation of ceramic fibers or particles which act as the load-bearing and abrasive member. There are excellent reviews on the tribology of aluminum–matrix composites which has been generally found to be a function of the applied load as well as the reinforcement volume fraction, particle size, and the shape and nature of the reinforcing phase. The matrix structure also influences the wear and friction behaviors of MMCs, so that the processing route and/or heat treatment conditions can enhance the wear resistance of these materials via their effects on the matrix microstructure, distribution of particles, porosity content, particle matrix bonding, and mechanical properties [7–11].

In this study, boron carbide (B_4C) powder was chosen as reinforcement because of its higher hardness (2900–3580 kg mm^{-2}) than the conventional and routinely used reinforcement such as SiC and Al_2O_3 [9].

The A356–B_4C composites have the potential to combine the high stiffness and hardness of B_4C with the ductility of Al and result in a strong low-density material [12].

The process of stir casting generally involves the admixture of ceramic particulate reinforcement with a molten metal matrix. The particulates are distributed and suspended in the molten metal via high energy mixing or another appropriate process. The suspended slurry is then cast as a foundry ingot, extrusion billet, or rolling bloom. This process is widely used for applications that require high production volumes and low cost [13].

In terms of preparing Al–B_4C composites, especially with a high B_4C content, the wettability of particles represents a very important issue which is poor at temperatures near the melting point of aluminum (660 °C). Thus,

M. O. Shabani (✉)
Materials and Energy Research Center (MERC),
P.O. Box 14155-4777, Tehran, Iran
e-mail: vahid_ostadshabany@yahoo.com

A. Mazahery
School of Metallurgy and Materials Engineering, University of Tehran, Tehran, Iran

attention was paid to the fact that B_4C powders coated with some of Ti compounds might have reasonable wettability with aluminum [14–18]. First, TiB_2 was coated on the surface of the B_4C particles via sol–gel processing and the A356-coated B_4C composite have been processed using stir casting. Then, the microstructure and wear properties of the composites have been experimentally investigated and finally the combination of finite element technique (FEM) (for discretization) and artificial neural network (ANN) is implemented for modeling of these properties. A neural network is a technique that seeks to build an intelligent computer program using models, which simulate working neurons in the human brain. The neural network is utilized in performing computations on computers, which includes different neurons joined to other neurons with synaptic weights to simulate the human brain [19–23].

Experimental procedure

The A356 aluminum alloy was employed as the matrix material. The conventional reinforcement materials for A356 are SiC and Al_2O_3. Due to the higher cost of B_4C powder relative to SiC and Al_2O_3, limited research has been conducted on B_4C-reinforced MMCs. In this study, the B_4C particles with average particle sizes of 1, 10, 21, 33, 42, and 55 μm were used as the reinforcements. The chemical composition of A356 and B_4C is represented in Tables 1, 2, respectively. The grain size of B_4C particles was analyzed using a Malvern laser size analyzer.

Titanium tetraisopropoxide (TTIP) was selected as a sol–gel precursor and diluted with ethanol. For coating of the titanium oxide, B_4C powders were dispersed in ethanol, stirred well, and then TTIP and distilled water were added to the stirred suspension. The processing was conducted at room temperature at a solution pH of 7.

Distilled water for hydrolysis was previously diluted by ethanol to inhibit the rapid hydrolysis of TTIP. For sol–gel processing, 0.1 M concentration of TTIP solution was prepared and added to 1 g of B_4C. The amount of water was adjusted to four times that of TTIP. The solution was then aged for 105 min at room temperature, with constant, gentle stirring. After the sol–gel process, the powders were paper-filtered and dried at 140 °C. When needed, sucrose was introduced in water solution. The powders were heat treated in a graphite crucible and under argon atmosphere. Figure 1 shows the heat treatment cycle that was implemented to eliminate the adsorbed water and to achieve a TiB_2 coating. The powders were analyzed by X-ray diffraction (XRD) and scanning electron microscopy (SEM). The results are represented in Figs. 2, 3, respectively.

For manufacturing of the MMCs, 2.5, 5, 7.5, 10, 12.5, and 15 vol% B_4C particles were used. The melt-particle slurry was stirred for 15 min at approximately 600 rev/min speed. Magnesium and strontium were added to Al–Si alloys to improve the wettability between aluminum matrix and reinforcing particles and modification of eutectic silicon particles, respectively.

Composite slurry was step cast into the CO_2-sand mold. Figure 4 shows side and top view of the model. The casting was gated from the side of the riser. It was then sectioned and samples were extracted from steps 1 to 5. The density

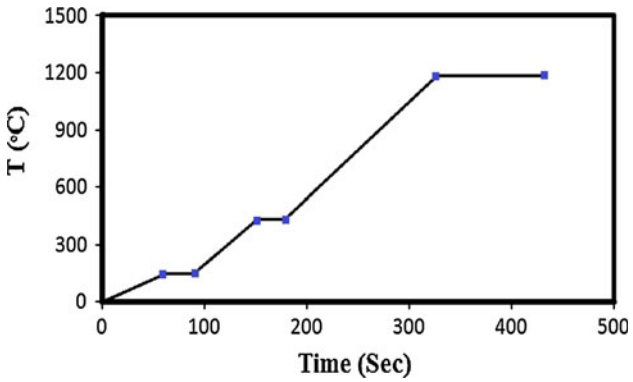

Fig. 1 Heat treatment cycle on B_4C powders after sol–gel process

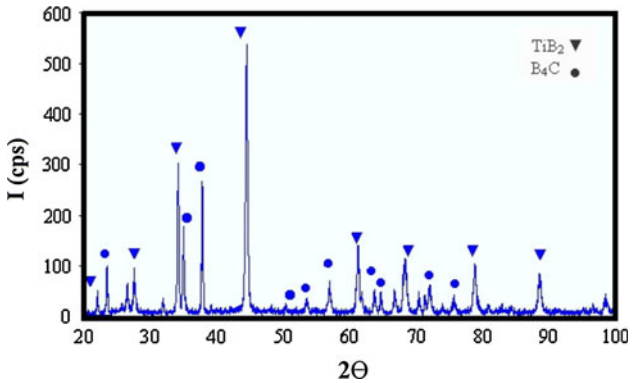

Fig. 2 XRD pattern of the coated B_4C powders

Table 1 Chemical composition of A356

Element	Al	Ni	Fe	Cu	Mg	Mn	Zn	Ti	Si
Wt%	Balance	0.05	0.1	0.001	0.38	0.02	0.02	0.01	7.5

Table 2 Chemical composition of B_4C

Total boron	77.50%
Total carbon	21.50%
Total iron	0.20%
Total B + C	98%

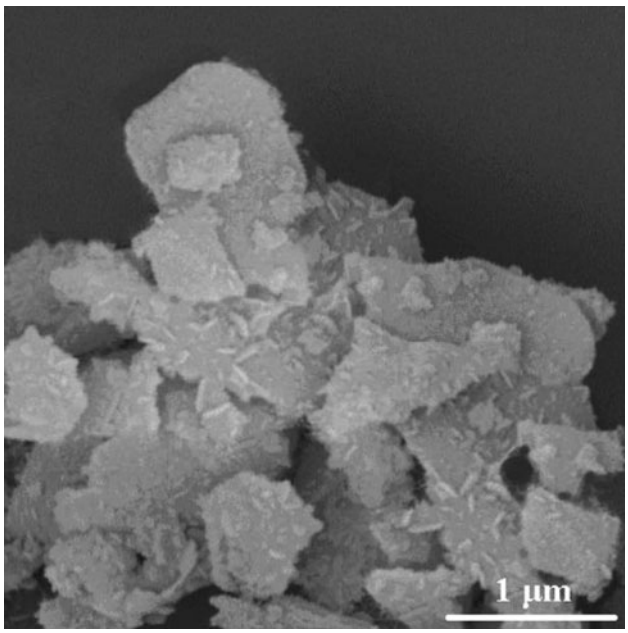

Fig. 3 SEM micrograph of the coated B_4C powders

of composites was measured using the liquid displacement technique following the Archimedes principle. The amount of porosity in the cast alloy and the composites was determined by comparing the measured density with that of their theoretical density using rule-of-mixtures.

The microstructures of the produced ingots were examined using an optical microscope to determine the distribution of the B_4C particles and the presence of porosity.

Specimens for the wear tests were solution treated at 540 °C for 4 h, quenched into warm water (40 °C) and then peak aged to T6 condition (155 °C for 9 h).

Dry sliding wear tests were performed using a pin-on-disk type wear apparatus. The slider disk was case hardened steel with 63 HRC to a depth of 3 mm. Composite were made into pin having 6 mm in diameter and 25 mm in height. The pins were put in contact with the slider. Both surfaces were polished to 0.5 pm and ultrasonically cleaned before testing. The tests were carried for different sliding distances under the normal load of 10 N. The weight losses were calculated from the differences in weight of the specimens measured before and after the tests to the nearest 0.1 mg using an analytical balance. A separate specimen was used to measure the weight loss for each sliding distance. The wear test was interrupted at regular intervals and the incremental weight loss of the sample was recorded. After each increment and before weighing, the disk and the pin were cleaned in an ultrasonic bath with acetone and hot wind dried below 100 °C. Results from the specimens with wear track geometries that were not compatible with the specification of ASTM standard G99-95 were discarded. All tests were performed at room temperature (21 °C, relative humidity 55%).

FEM and ANN

In this research, wear properties are considered to be related to cooling rate, temperature gradient, volume percentage of B_4C (0, 2.5, 5, 7.5, 10, 12.5, and 15), average particle size of B_4C (1, 10, 21, 33, 42, and 55 μm), and sliding distance (0, 200, 400, 600, 800, 1000, 1200, 1400, 1600, 1800, and 2000 m). The method couples thermal and solute diffusion with the governing equations for modeling of heat transfer during solidification as follows [24]:

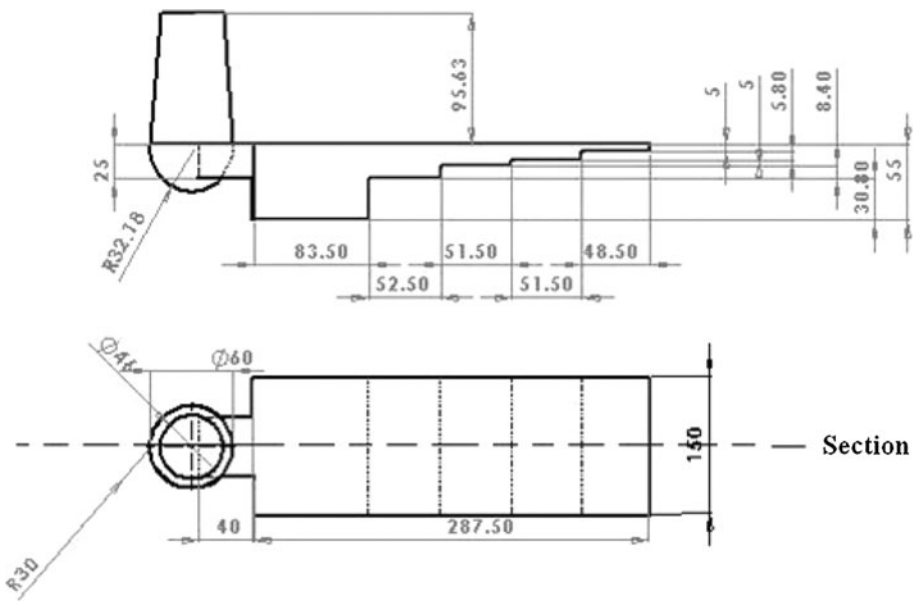

Fig. 4 Side and top view of the model

$$\rho C_p \frac{\partial T(x,y,z,t)}{\partial t} = K\nabla^2 T(x,y,z,t) \quad (1)$$

$$C_P = \begin{cases} C_{P(\mathrm{L})} & T > T_\mathrm{L} \\ C_{P(\mathrm{SL})} + \frac{L \cdot f_\mathrm{s}}{T_\mathrm{L} - T_\mathrm{S}} & T_\mathrm{S} \le T \le T_\mathrm{L} \\ C_{P(\mathrm{S})} & T < T_\mathrm{S} \end{cases} \quad (2)$$

$$C_{P(\mathrm{SL})} = C_{P(\mathrm{S})} \cdot f_\mathrm{s} + C_{P(\mathrm{L})} \cdot f_\mathrm{L}, \quad (3)$$

where ρ is density, C_p heat capacity, K heat diffusion coefficient, L latent heat.

The evolution of solid fraction (f_s) is given by the Scheil equation [24]:

$$f_\mathrm{s} = 1 - \left(\frac{T_\mathrm{L} - T}{T_\mathrm{L} - T_\mathrm{S}}\right)^{1/(k_0 - 1)}. \quad (4)$$

Based on the above transient temperature model, the FEM method is used for discretization and to calculate the transient temperature field of quenching. Since it is almost at $T{=}T_\mathrm{S} + 0.1(T_\mathrm{L} - T_\mathrm{S})$ that final structure and latent heat are obtained, the cooling rate and temperature gradient in dendrite tip are required.

$$R = T(i,j,k,t) - T(i,j,k,t+1) \quad (5)$$

$$G = |(T(i+1,j,k,t) - T(i,j,k,t))|, \quad (6)$$

where k_0 is solute partition coefficient, R cooling rate, and G temperature gradient.

There are several variables that have an effect on the ANN training. These variables are the number of training data points, network size (number of hidden layer and neurons in each layer), and number of training iterations or epoch. To find the best set of these variables and parameters, all of those should be varied and then the best combinations are chosen. Also the ANNs can be judged by various parameters such as the mean square error (MSE) and mean absolute error (MAE) as follows [25–28]:

$$\mathrm{MSE} = \left(\frac{1}{QN_0}\sum_{m=1}^{Q}\sum_{n=1}^{N_0}|d_n(m) - y_n(m)|\right)^2 \quad (7)$$

$$\mathrm{MAE} = \sum\left|\frac{x-y}{n}\right|, \quad (8)$$

where N_0 is the number of output, Q the number of training sets, d desired output, and y the network output and where $x = X - X'$, X is the target output and X' the mean of X, $y = Y - Y'$, Y is the network output and Y' the mean of Y. In this investigation, the MSE was used to evaluate the performance of model.

The ANN architecture is shown in Fig. 5. A total dataset of 35 samples was used to learn the proposed ANN. This dataset was obtained from step casting process. Among them, 27 of these points are used in training process and 8 used in validation process.

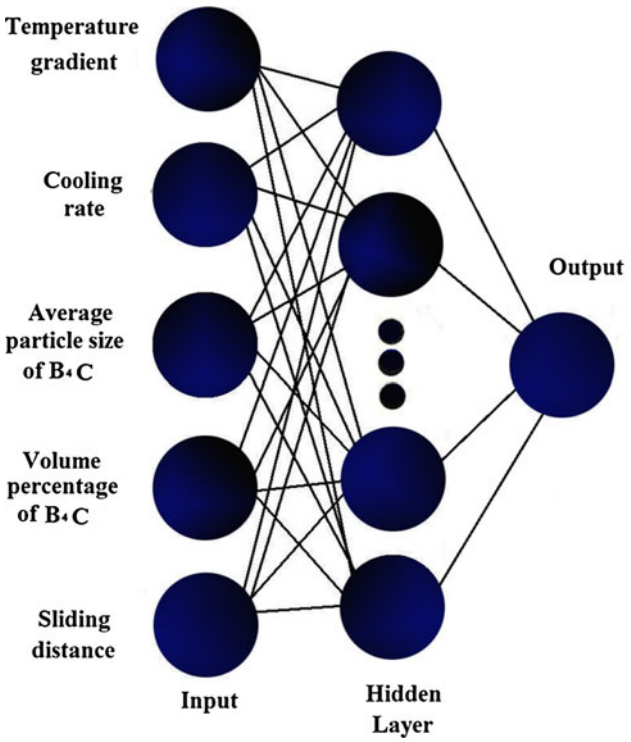

Fig. 5 Schematic representation of the neural network architecture

The network has been trained with Levenberg–Marquardt algorithm. This training algorithm has been selected due to its high accuracy in similar function approximation. The number of neurons in the input and the output layers are determined by the number of input and output variables, respectively. In order to find an optimal architecture, different number of neurons in the hidden layer was considered and MSE error for each network was calculated [26–30]. For the training problem, the following parameters were found to give good performance and rapid convergence: two of five input nodes were obtained from FEM method namely cooling rate (K/s), temperature gradient (K/m), plus three other nodes including volume percentage of B_4C, average particle size of B_4C and sliding distance. Also, once the single output neuron is variation of porosity and the other time it is weight loss. Neural network with one output seems to present better results than the one with two outputs. Two outputs required simultaneous prediction by one model and the weights were adjusted to make the minimum error sum at each learning iteration. The experimental results can not really show the best relationship between each individual output and its inputs.

Results and discussion

The variation of porosity with the B_4C particles size and B_4C content are shown in Fig. 6a, b, respectively. It is

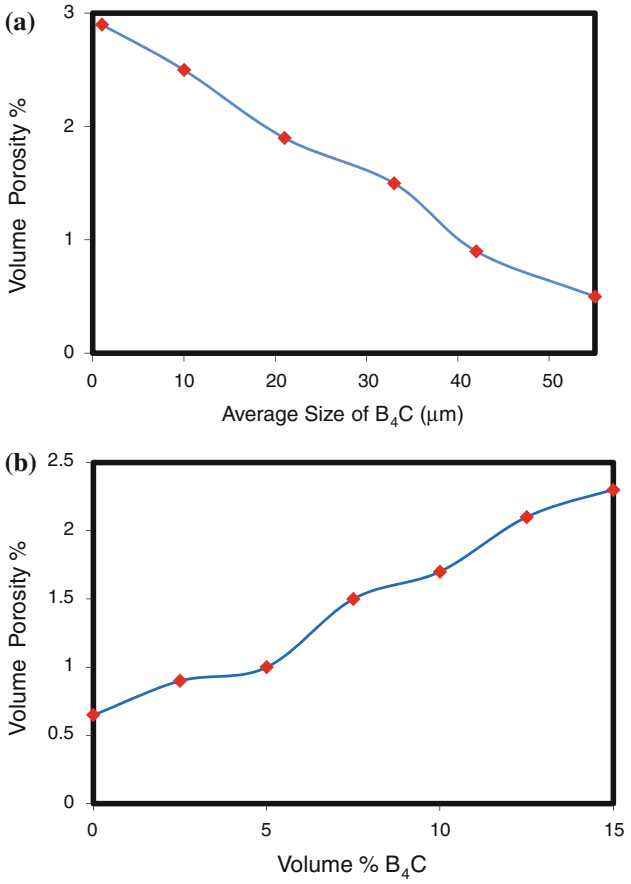

Fig. 6 Variations of porosity of the composites as a function of **a** average size of B_4C for a fixed particle content of 7.5 vol% and **b** B_4C content for fixed particle size of 33 μm

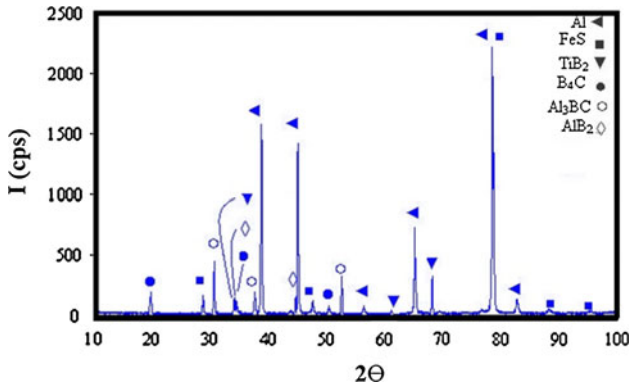

Fig. 7 XRD pattern of the composite with 10 vol% coated B_4C

shown that for a fixed B_4C particles content (7.5 vol%), the porosity of composite samples increase with decreasing size of B_4C particles. Figure 6b shows that increasing amount of porosity is observed with increasing the volume fraction for composites containing fixed size of B_4C particles (33 μm). This trend is also reported by the early studies [1, 31]. This is attributed to pore nucleation at the B_4C particulate sites (porosity associated with individual particle) and to hindered liquid metal flow due to more particle clustering (porosity associated with the particle clusters) [31–33].

The XRD pattern of the composite with 10 vol% coated B_4C is displayed in Fig. 7. It can be seen that Al, B_4C, and TiB_2 are present in the sample. The XRD results also revealed the presence of Al_3BC and AlB_2 phases. The maximum solubility of boron and carbon in aluminum is relatively low (0.1 wt% and a few tenths of a ppm), thus these two elements rapidly dissolute and saturate the melt. Subsequently, AlB_2 nucleates on impurity seeds from the supersaturated melt, while the Al_3BC phase nucleates at the B_4C surface. Growth continues via a classical dissolution–precipitation mechanism [12].

Figure 8 shows a SEM micrograph of a coated B_4C particle throughout the Al matrix. In order to investigate the composition of this particle, several X-ray maps were carried out, confirming the accuracy of previous speculation (Fig. 8a, b, c). The X-ray maps prove the existence of boron and carbon in the particle spot.

Figure 9 shows optical micrograph of the metal matrix composite. This figure clearly shows that α-aluminums are predominately present in the as-cast A356 and A356/B_4C composite alloys. Because of the casting process, the B_4C particles were distributed between the dendrite branches and were frequently clustered together, leaving the dendrite branches as particle-free regions in the material. The presence of eutectic silicon on B_4C particles indicates heterogeneous nucleation of eutectic silicon on B_4C particles and also the role of B_4C particles as a physical barrier for growing of eutectic silicon during solidification [34, 35].

Figure 10 gives a general picture of the effect of B_4C particles on the wear rates regime of composites containing different volume percentages and sizes. It is clear from these graphs that the weight losses of the composites are less than that of unreinforced alloy. According to the differences in wear rates of the unreinforced and reinforced alloys, two separate wear rate regimes were identified by lower curves and higher curves indicating low and high wear rate, respectively. The results indicate that all the composite samples reinforced with 1 μm B_4C particles show the high wear rate, regardless of the particle volume fraction (Fig. 10a). However, only some of composite samples reinforced with 21 μm particles and none of the samples of 55 μm display this type of wear regime (Fig. 10b, c). It is believed that the particles act as load-bearing elements. Thus, the weight loss decreases with increasing the B_4C volume percentage. Moreover, since

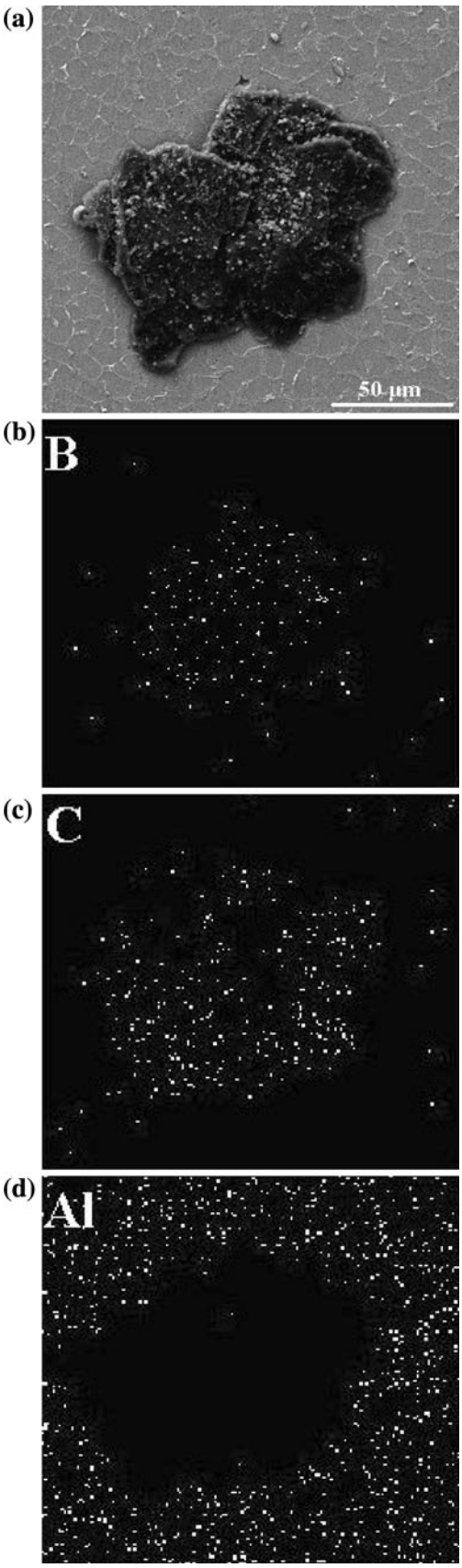

◀ **Fig. 8** **a** B_4C particle throughout the Al matrix; x-ray maps, showing the elements in picture, **b** boron, **c** carbon, and **d** aluminum

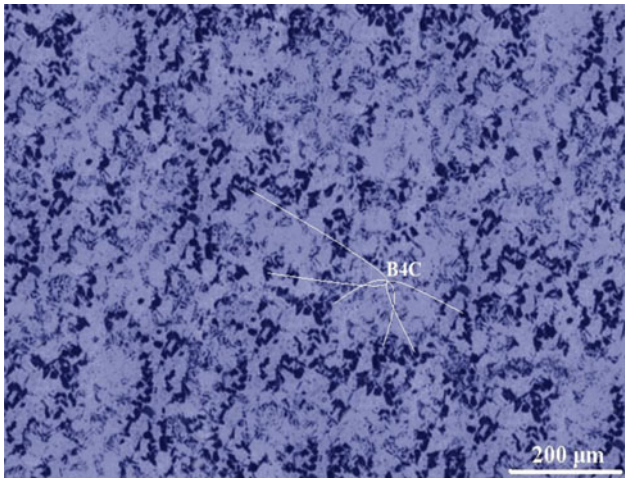

Fig. 9 Typical optical micrograph of the composite with 12.5 vol% coated B_4C (33 μm)

B_4C is brittle in nature, it gets fragmented preferentially and redistributed on the surface. This helps to relieve part of the shear strains built up in the subsurface [4, 7, 9].

The SEM micrographs of the worn surfaces reveal that excessive plastic plowing and cutting can be seen in the unreinforced Al alloy (Fig. 11a). The rough and smooth regions are distinguished on the worn surface of the composites similar to the unreinforced alloy (Fig. 11b). In addition, grooves were shallow in the case of composites. Cavities or craters of rough regions indicate that locally adhesive wear and fine grooves or plowing of smooth regions suggest that locally abrasive wear were dominant mechanisms.

It can be noted that volume fraction and average size of B_4C particles play the main role on wear behavior of composites. The highest applied load which can be supported by the B_4C particles is known as the transient load. It was reported in the previous research that the particles act as load-bearing components when the nominal load is lower than transient load (low wear rate regime). A prerequisite for this type of wear is that the B_4C particles should remain intact during wear to support the applied load and act as effective abrasive elements. When the applied load induces stresses that exceed the fracture strength of carbide particles, the particles fracture and largely lose their effectiveness as load-bearing components. The shear strains are then transmitted to the matrix alloy and wear proceeds by a subsurface delamination process (high wear rate regime). In this case, the lower ductility of Al–B_4C composites appears to control the wear rates rather than the hardness of particles, resulting in wear rates almost similar to

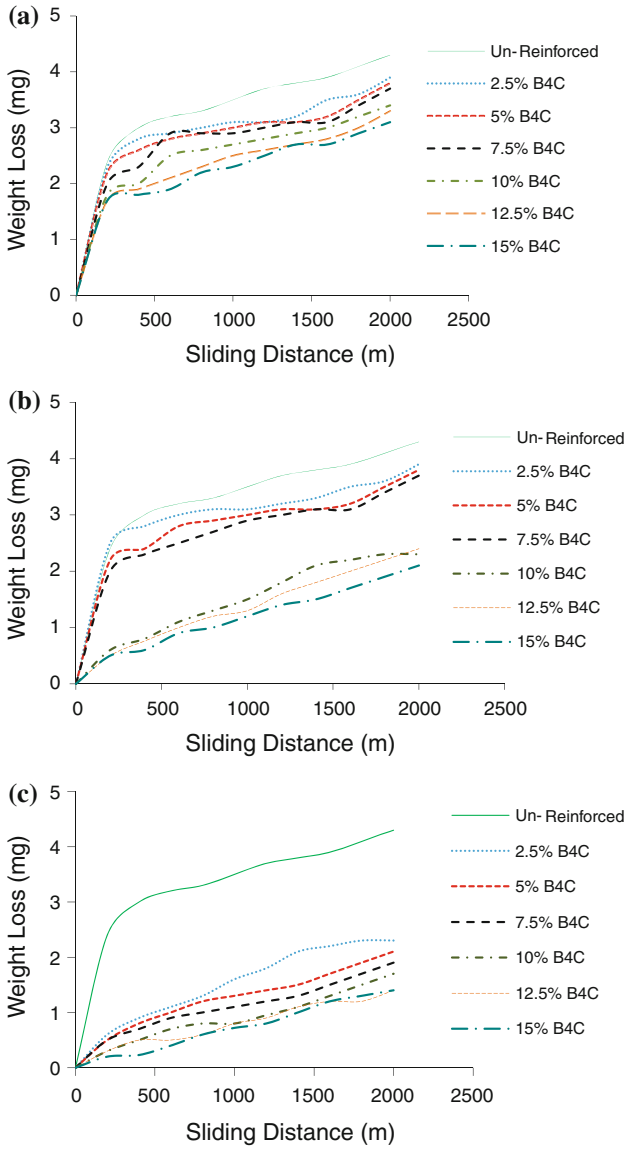

Fig. 10 Typical variations of wear loss as a function of sliding distance for different average sizes of the B_4C particles: **a** 1 μm, **b** 21 μm, and **c** 55 μm

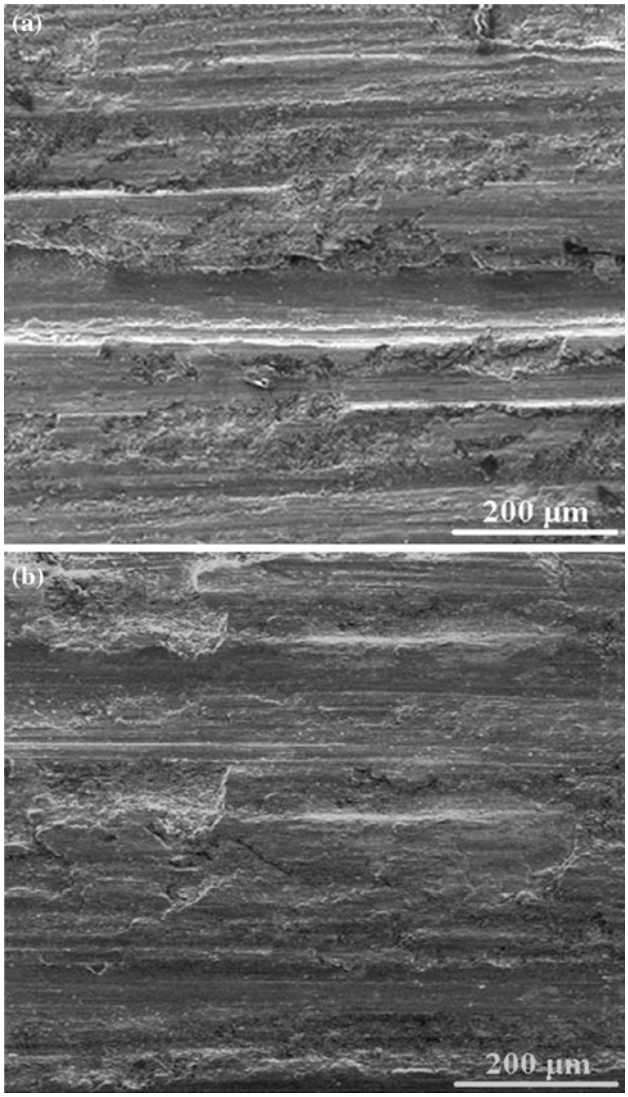

Fig. 11 SEM micrograph of worn surfaces: **a** A356 and **b** A356–7.5% B_4C particles (22 μm)

those observed in aluminum–silicon alloys without B_4C reinforcement.

It is reported that the debris of the composites with low wear rate are associated with the formation of more iron-rich layers on the contact surfaces. During sliding wear, iron, and possibly other alloying elements, from the steel counterface are transferred to the surface of the composites. The iron-rich transfer layers help the B_4C particles to remain unbroken during wear and act as load-bearing elements. It is also reported that iron is oxidized during this process and oxide layers, in particular Fe_20_3 layers generated during wear, act as solid lubricants and help to reduce the wear rates [3, 36–38].

The number of hidden layers and neurons within each hidden layer can be varied based on the complexity of the problem and the data set. The neuron number in the hidden layer can be found experimentally. The optimal configuration was based upon minimizing the difference between the neural network predicted values and the desired outputs. In Fig. 12, MSE error values are computed and given at the end of training process for various neurons in the hidden layer. According to this figure, the MSE error of the predictions for the entire data (train and test data combined) is:

$$\text{Variation of porosity} = 0.044(\text{with 6 neurons in hidden layer})$$

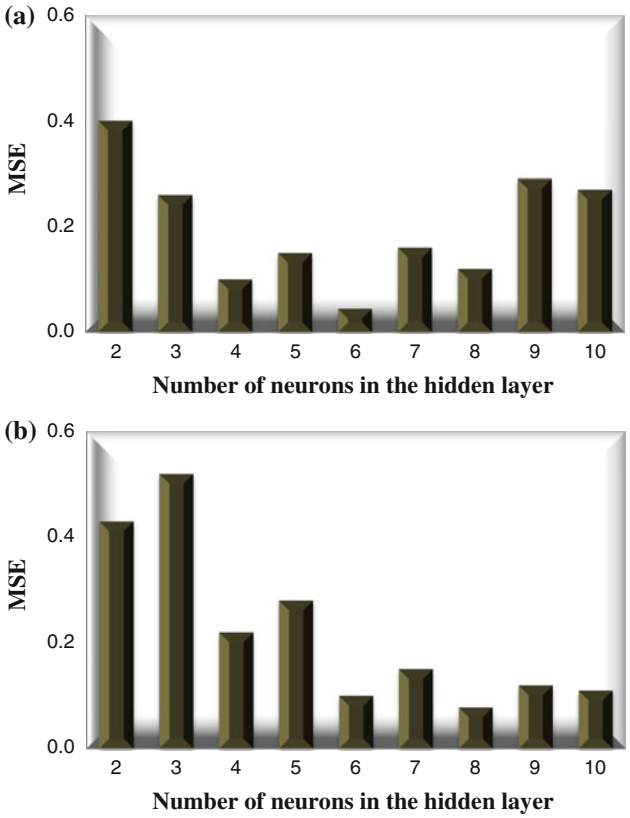

Fig. 12 MSE error values for various neuron in the hidden layer: **a** variation of porosity and **b** weight loss

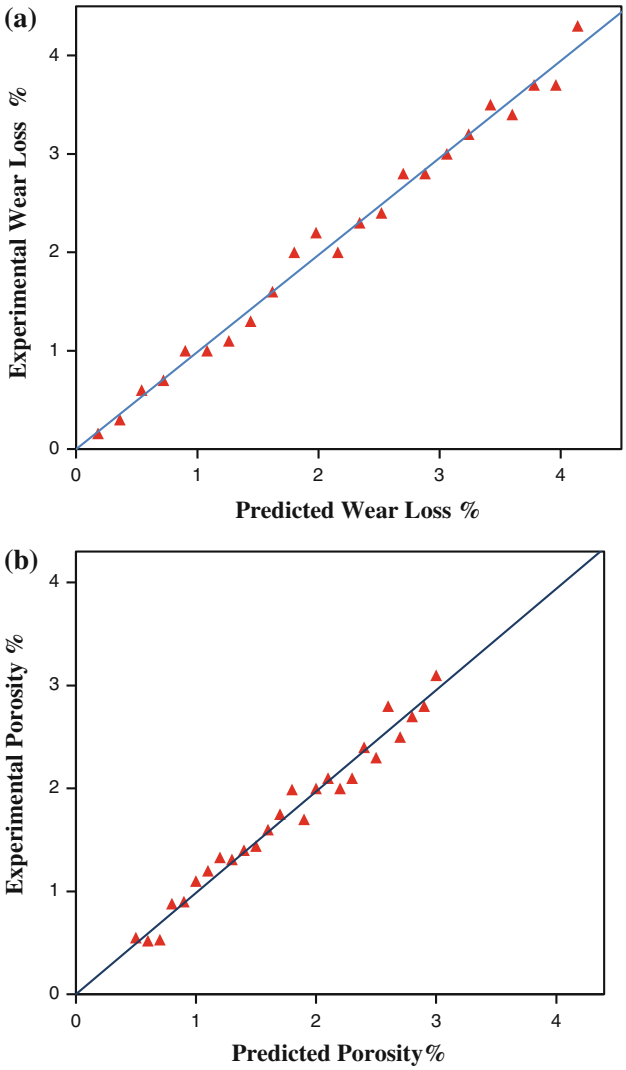

Fig. 13 Comparison between the experimental and predicted values: wear loss (**a**) porosity (**b**)

$$\text{Weight loss} = 0.078(\text{with 8 neurons in hidden layer}).$$

The model is verified against the cases in the test data file, which are independent of the ones in the train data file. The predicted results are plotted versus the experimental results. Although the use of this model may lead to a higher performance error for the training datasets, the error for the test datasets is reduced which is an indication of higher ability of the network to predict more precise results from unseen patterns. Comparison between the experimental and predicted values of porosity content and weight loss is displayed in Fig. 13. The remarkable agreement between the experimental and predicted values implies that the ANN model can be used to predict the mechanical properties.

Conclusions

In this study, the B_4C powders were coated with TiB_2 and incorporated into the aluminum matrix by a mechanical stirrer. XRD analyses detected the combination of various phases including B_4C, TiB_2, Al_3BC, and AlB_2. Microstructure characterization revealed an uniform distribution of the coated B_4C particles between the dendrite branches. The experimental wear rates results of the unreinforced and reinforced alloys show two separate wear rate regimes. It is observed that the presence of B_4C particles could shield the matrix and silicon phases from directly experiencing the applied load and reduce the weight loss during the wear test. The ANN modeling of wear properties was developed to predict the tribological behavior of A356-reinforced coated B_4C composites. The prediction of this modeling was found to be in good agreement with experimental data. The FEM was also implemented to calculate the transient temperature field of quenching.

References

1. Samuel AM, Gotmare A, Samuel FH (1995) Compos Sci Technol 53:301
2. Chung S, Hwang BH (1994) Tribol Int 27(5):307
3. Mazahery A, Shabani MO, Salahi S (2011) Materials science and Technology. Maney Publishing, Leeds
4. Lim SC, Gupta M, Ren L, Kwok JKM (1999) J Mater Process Technol 89–90:591–596
5. Bindumadhavan PN, Chia TK, Chandrasekaran M, Wah HK, Lam LN, Prabhakar O (2001) Mater Sci Eng A 315:217
6. Roy M, Venkataraman B, Bhanuprasad VV, Mahajan YR, Sundararajan G (1992) Metall Trans A 23:2833
7. Skolianos S, Kattamis TZ (1993) Mater Sci Eng A 163:107
8. Surappa MK, Prasad SV, Rohatgi PK (1982) Wear 77:295
9. Bindumadhavan PN, Wah HK, Prabhakar O (2001) Wear 248: 112
10. Kwok JKM, Lim SC (1999) Compos Sci Technol 59:55
11. Das S, Mondal DP, Dixit G (2001) Metall Mater Trans A 32:633
12. Viala JC, Bouix J, Gonzalez G, Esnouf C (1997) J Mater Sci 32: 4559. doi:10.1023/A:1018625402103
13. Evans A, Marchi CS, Mortensen A (2003) Metal matrix composites in industry: an introduction and a survey. Kluwer Academic Publishers, Dordrecht
14. Blumenthal WR, Gray GT III, Claytor TN (1994) J Mater Sci 29:4567. doi:10.1007/BF00376280
15. Pyzik AJ, Aksay IA, Sarikaya M (1986) Mater Sci Res 21:45
16. Pyzik AJ, Aksay IA (1989) Processing of ceramic and metal matrix composites. Pergamon Press, New York, p 269
17. Pyzik AJ, Beaman DR (1995) J Am Ceram Soc 78:305
18. Rhee SK (1970) J Am Ceram Soc 53:386
19. Hassan AM, Alrashdan A, Hayajneh MT, Mayyas AT (2009) J Mater Process Technol 209:894
20. Karimzadeh F, Ebnonnasir A, Foroughi A (2006) Mater Sci Eng A 432:184
21. Altinkok N, Koker R (2004) Mater Des 25:595
22. Singh SK, Mahesh K, Gupta AK (2010) Mater Des 31:2288
23. Lisboa PJ, Taktak AFG (2006) Neural Netw 19:408
24. Ostad Shabani M, Mazahery A (2011) Int J Appl Math Mech 7:89
25. Rashidi AM, Eivani AR, Amadeh A (2009) Comput Mater Sci 45:499
26. Mousavi Anijdan SH, Bahrami A, Madaah Hosseini HR, Shafyei A (2006) Mater Des 27:605
27. Hwang R-C, Chen Y-J, Huang H-C (2010) Expert Syst Appl 37:3136
28. Fratini L, Buffa G, Palmeri D (2009) Comput Struct 87:1166
29. Hamzaoui R, Cherigui M, Guessasm S, ElKedim O, Fenineche N (2009) Mater Sci Eng B 163:17
30. Reddy NS, Prasada Rao AK, Chakraborty M, Murty BS (2005) Mater Sci Eng A 391:131
31. Lloyd DJ, Chamberian B (1988) Cast reinforced metal composites. ASM, Illinois, p 263
32. Ray S (1988) In: Proceedings of the survey on fabrication methods of cast reinforced metal composites, p 77, ASM/TMS, 1988
33. Rana F, Stefanescu DM (1989) Metall Mater Trans A 20:1564
34. Nagarajan S, Dutta B (1999) Compos Sci Technol 59:897
35. Zhou W, Xu ZM, Mater J (1997) Process Technol 63:358
36. Ludema KC (1984) Wear 100:315
37. Lim SC, Ashby MF (1987) Acta Metall 35:l
38. Razavizadeh K, Tyre TS (1982) Wear 79:325